BIOCHEMISTRY
including biophysical chemistry & molecular biology

Article

pubs.acs.org/biochemistry

Aggregation Behavior of Chemically Synthesized, Full-Length Huntingtin Exon1

Bankanidhi Sahoo,[†] David Singer,[‡] Ravindra Kodali,[†] Thole Zuchner,[‡] and Ronald Wetzel*[,†]

[†]Department of Structural Biology and Pittsburgh Institute for Neurodegenerative Diseases, University of Pittsburgh School of Medicine, Pittsburgh, Pennsylvania 15260, United States

[‡]Institute of Bioanalytical Chemistry, Faculty of Chemistry and Minerology, Center for Biotechnology and Biomedicine, Leipzig University, Leipzig 04103, Germany

ABSTRACT: Repeat length disease thresholds vary among the 10 expanded polyglutamine (polyQ) repeat diseases, from about 20 to about 50 glutamine residues. The unique amino acid sequences flanking the polyQ segment are thought to contribute to these repeat length thresholds. The specific portions of the flanking sequences that modulate polyQ properties are not always clear, however. This ambiguity may be important in Huntington's disease (HD), for example, where *in vitro* studies of aggregation mechanisms have led to distinctly different mechanistic models. Most *in vitro* studies of the aggregation of the huntingtin (HTT) exon1 fragment implicated in the HD mechanism have been conducted on inexact molecules that are imprecise either on the N-terminus (recombinantly produced peptides) or on the C-terminus (chemically synthesized peptides). In this paper, we investigate the aggregation properties of chemically synthesized HTT exon1 peptides that are full-length and complete, containing both normal and expanded polyQ repeat lengths, and compare the results directly to previously investigated molecules containing truncated C-termini. The results on the full-length peptides are consistent with a two-step aggregation mechanism originally developed based on studies of the C-terminally truncated analogues. Thus, we observe relatively rapid formation of spherical oligomers containing from 100 to 600 HTT exon1 molecules and intermediate formation of short protofibril-like structures containing from 500 to 2600 molecules. In contrast to this relatively rapid assembly, mature HTT exon1 amyloid requires about one month to dissociate *in vitro*, which is similar to the time required for neuronal HTT exon1 aggregates to disappear *in vivo* after HTT production is discontinued.

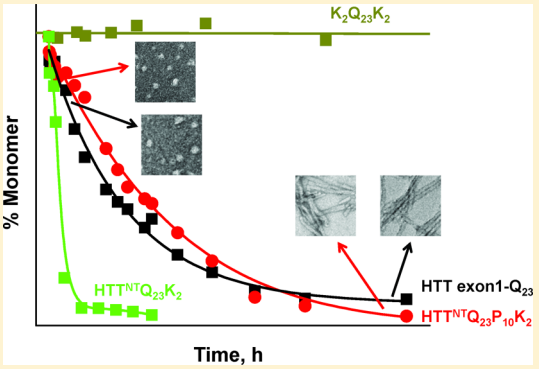

Huntington's disease[1,2] (HD) is one of 10 known expanded CAG repeat diseases,[3,4] autosomal dominant genetic disorders in which polyglutamine (polyQ) sequences above characteristic repeat lengths in specific disease proteins trigger neurodegeneration. The molecular mechanism of HD has not been elucidated, but the consensus is that polyQ expanded forms of N-terminal fragments, typified by the translation product of the huntingtin (HTT) gene's first exon, are susceptible to aberrant folding behaviors that somehow interfere with normal neuronal function or survival. This protein fragment, which has become known as HTT exon1, can be generated in the cell either by proteolytic fragmentation of the full-length HTT protein[5] or by translation of an alternatively spliced version of HTT mRNA.[6] Animal models based on overexpression of HTT exon1 exhibit robust neurodegenerative phenotypes.[7]

Regardless of polyQ repeat length, HTT exon1 itself is not stably folded but rather is an amalgam of three sequence-defined segments (Figure 1), each of which exhibits aspects of intrinsically disordered protein[8] (IDP) behavior.[9] The N-terminal 16 or 17[9] amino acid segment, HTT^{NT}, is disordered in solution in the monomeric state[10] but takes on α-helical structure when it self-associates[11] and when it interacts with membranes.[12] The central polyQ segment exists in the monomer in an energetically favored compact coil state[9,13−15] consisting of fluctuating short segments of coil, α, and β structure in which glutamine side chain amides spend significant time H-bonded to main chain amide groups.[16] The C-terminal proline-rich domain (PRD), consisting of runs of P_{10} and P_{11} alternating with short segments of mixed, Pro-rich sequence, favors polyproline type II (PPII) structure but is not expected to exhibit a single, strongly favored conformation.[9,15] Whether and how these three disordered sequence elements interact with each other, through the peptide backbone and through space, to define or modulate the solution properties of HTT exon1 is a challenging problem that is only beginning to be explored.[9,17,18]

Under the umbrella of opinion that HD is a protein misfolding disease, there is a wide range of ideas about the nature of the toxic misfolded species.[9,15] Some research has been interpreted to indicate that repeat expansion favors the

Received: March 10, 2014
Revised: May 31, 2014
Published: June 12, 2014

   dx.doi.org/10.1021/bi500300c | *Biochemistry* 2014, 53, 3897−3907

$K_2Q_NK_2$	K_2-Q_N-K_2
$HTT^{NT}Q_NK_2$	MATLEKLMKAFESLKSF-Q_N-K_2
$HTT^{NT}Q_NP_{10}K_2$	MATLEKLMKAFESLKSF-Q_N-$P_{10}K_2$
HTT exon1	MATLEKLMKAFESLKSF-Q_N-P_{11}QLPQPPPQAQPLLPQPQP$_{10}$GPAVAEEPLHRP

Figure 1. Sequences of peptides used in this study.

time-dependent formation of an alternatively folded state of polyQ in which the average monomer in solution possesses β-hairpin structure.[19,20] These ideas are hard to reconcile, however, with our understanding of the energetic features of the polyQ monomer conformational landscape,[9,14,16,21] and there are reasonable alternative interpretations of the supporting data.[15,22,23] In contrast, other results have been interpreted to implicate the repeat length and time-dependent formation of some kind of aggregated state of HTT exon1 as potential toxic entities.[24−26] These ideas are consistent with the well-established existence of large HTT exon1 containing inclusions in neurons of affected individuals[27] and in cell[28] and animal models,[29] and in the similarities between the polyQ repeat length dependences of disease risk and age-of-onset[30] and *in vitro*[13,31] and *in vivo*[32] aggregation behavior. Although compelling evidence has been presented that the large inclusions that appear late in the cellular aggregation time course are more likely to be protective than toxic,[33] it is now clear that smaller amyloid fibrils[34] as well as more difficult to detect nonamyloid aggregates[9,35−38] are also generated in cell and animal models. The undiminished feasibility of the aggregation hypothesis makes it imperative that we continue to work to understand molecular mechanisms of aggregation and how different segments of HTT exon1 act and interact to propel or retard these mechanisms.

Data on HTT exon1 self-assembly mechanisms and products have been generated using molecules from two different types of sources. One source generates essentially full-length HTT exon1 made in bacterial[22,39−42] or mammalian[43] cell culture, using a fusion protein approach that helps retain the aggregation-prone product in solution in the cell but leads to compromises in the integrity of the HTT exon1 N-terminus when the fusion partner is removed. The other major approach is to use peptides obtained by solid phase peptide synthesis, which, however, is limited by the length of peptides that can be conveniently synthesized. For this reason, most synthetic peptide studies have been constrained to relatively short (no longer than the low 40s) polyQ repeat lengths and truncated C-termini.[10,44−50] Thus, the choice of the source of HTT exon1 analogues for *in vitro* studies of self-assembly and toxicity is guided in part by one's perception of the relative importance of maintaining absolute sequence integrity in the N-terminus vs the C-terminus.

Previous studies using chemically synthesized HTT exon1 fragments led to development of a detailed mechanism (Figure 2) for how peptides in this class self-assemble.[9−11,15,46,48] The presence of a functioning HTT^{NT} sequence leads to a dominant pathway (A) featuring early formation of oligomers (b, c, d) consisting of superassembled tetramers that are themselves held together by bundling of α-helical HTT^{NT} segments (green cylinders). Oligomer formation leads to very high local concentrations of compact coil polyQ segments (orange), which favors stochastic amyloid nucleation events (e) that trigger fibril elongation (f). This mechanism is supported by the identification of early nonamyloid oligomers held together by HTT^{NT} interactions,[10] the observation of well-behaved

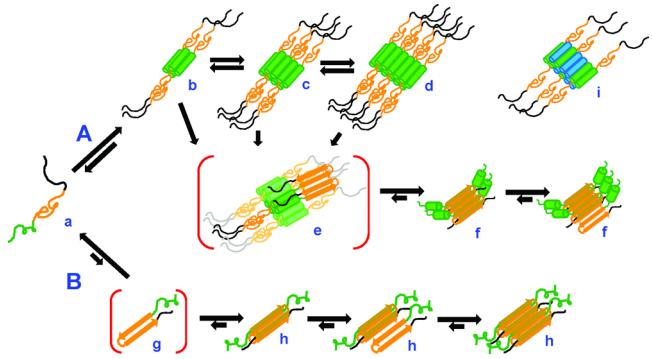

Figure 2. Mechanisms of polyglutamine amyloid assembly. Monomeric HTT exon1 analogues (a) can assemble into polyQ-core amyloid by two mechanisms, nominally in competition.[46] Pathway A. Monomers assemble into tetramers via concerted α-helix formation and bundling of the N-terminal 16−17 amino acid segment HTT^{NT} (green) (b−d). Non-β oligomers assemble via poorly understood self-association of tetramers. This reversible oligomerization brings the polyQ chains (orange) close together in space at a very high local concentration, facilitating sporadic amyloid nucleation (e), which leads to amyloid elongation (f) into fibrils. The proline rich C-terminal segment (black) tends to favor PPII conformations throughout. Pathway B. If pathway A is compromised, for example, by coassembly with HTT^{NT} peptides (i) (see text), amyloid nucleation can still occur by the classical nucleated growth polymerization type mechanism previously described for simple polyQ sequences.[56,74] Reproduced from ref 46. Copyright 2012 American Chemical Society.

tetramers and octamers requiring the presence of HTT^{NT},[11] the ability of HTT^{NT} with or without added polyQ to form α-helix in a concentration-dependent manner,[11] and the ability of peptides consisting only of the HTT^{NT} segment to inhibit nucleation by coassembling into mixed oligomers that reduce the local polyQ concentration[48] (Figure 2i). Interestingly, when such inhibitors compromise the HTT^{NT}-mediated pathway (A), the nucleation mechanism of polyQ amyloid reverts to the less efficient pathway (B) favored by simple polyQ peptides.[46] In contrast to the mechanism shown in Figure 2, studies based on recombinant HTT exon1 led to a proposed alternative mechanism in which non-β oligomers are assembled primarily via polyQ interactions.[51,52] It is not clear whether the stark differences in these mechanistic proposals and the data on which they are based stem from the structural differences between the HTT exon1-like molecules being studied, their synthetic source, the detailed methods used to initiate and monitor reactions, or other factors.

Previously, some of us reported the solid phase chemical synthesis of full-length HTT exon1 molecules containing repeats of 23 and 42 glutamine residues.[53] The availability of these well-defined molecules served as the basis for the direct comparative studies reported here, allowing us to cleanly focus on the question of the relative importance of sequences within the proline-rich domain (PRD) downstream from the first 10 prolines. The results confirm a number of key points in the mechanism devised previously based on work with C-terminally truncated HTT exon1 peptides, suggesting that for many

dx.doi.org/10.1021/bi500300c | *Biochemistry* 2014, 53, 3897−3907

studies C-terminally truncated HTT exon1 analogues can provide information relevant to the behavior of full-length HTT exon1. The results also provide new information on the role of the PRD on aggregate assembly and stability.

EXPERIMENTAL PROCEDURES

Materials and General Methods. Preparation of purified full-length HTT exon1 peptides has been described.[53] Other synthetic peptides were obtained from the Keck Biotechnology Center at Yale University and were purified by reverse phase HPLC as described.[11,54] Mass spectrometry evaluation of the purified peptides,[55] which run as a single peak in analytical reverse phase HPLC, gave absolute purities in the 70−90% range. In addition, if peptides containing only single deletions or insertions of glutamine or proline are included, purities rise to the following levels: $HTT^{NT}Q_{23}P_{10}K_2$, 97%; HTT exon1-Q_{23}, 94%; $HTT^{NT}Q_{42}P_{10}K_2$, 86%; HTT exon1-Q_{42}, 93%. Peptides were disaggregated in a mixture of trifluoroacetic acid and hexafluoroisopropanol immediately prior to initiating aggregation kinetics analyses, as described previously.[54,56] The effectiveness of the disaggregation was confirmed in each case by the absence of aggregates and the absence of scatter above that of buffer in the zero minute time points of the aggregation reactions. Aggregation kinetics were monitored by determining for each time point the amount of monomeric peptide remaining in solution, using an HPLC sedimentation assay described previously.[54] Determination of the equilibrium concentration of monomer in amyloid formation reactions (C_r) was accomplished by using the HPLC sedimentation assay to determine monomer concentrations at each time. Reverse reactions were initiated by diluting part of a nearly complete aggregation reaction in PBS and incubating, as described previously.[54,56] FTIR spectroscopy was conducted on isolated aggregates, on an ABB Bomem FTIR spectrometer, as described.[11] Dynamic light scattering measurements were conducted on aggregation reaction time points on a Wyatt DynaPro, as described.[11] Negative stain electron microscopy was conducted on aggregation reaction time points using a Tecnai T12 microscope, as described.[11] Analysis of dimensions of selected particles in the EM was done with the help of NIH ImageJ software (http://imagej.nih.gov/ij/).

RESULTS

Aggregation Kinetics. To examine the roles of the polyQ flanking sequences in HTT exon1-like peptides, we studied the peptide sequences shown in Figure 1, where the polyQ repeat length is either 23 or 42. The spontaneous aggregation kinetics curves of PBS solutions of rigorously disaggregated samples of these peptides are shown in Figure 3. As described previously,[56] $K_2Q_{23}K_2$ (green star) aggregates imperceptibly at 40 μM even after 1000 h (Figure 3A). In contrast, aggregation of $HTT^{NT}Q_{23}K_2$ (green square) at a 10-fold lower concentration of 4 μM is essentially complete after 75 h. As previously described,[10] the addition of a P_{10} sequence to generate $HTT^{NT}Q_{23}P_{10}K_2$ slows aggregation in comparison to $HTT^{NT}Q_{23}K_2$, so that it takes about 1000 h for a 13 μM solution of this peptide to aggregate to completion (red filled circle). Importantly, the aggregation kinetics time course of an 11 μM solution of full-length HTT exon1-Q_{23} (■) is very similar to that of $HTT^{NT}Q_{23}P_{10}K_2$. The slight difference in shape, which appears to be well within the error bars of the kinetics measurements (Figure 3A), may be due to a combination of differences in nucleation efficiency, elongation rate constants, and critical concentration (see below).

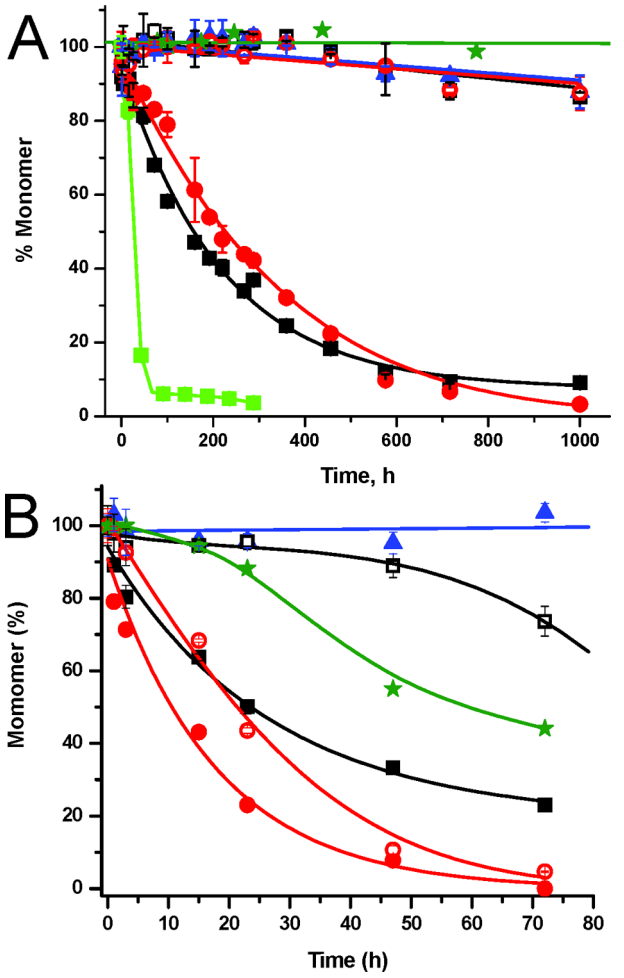

Figure 3. Kinetics of spontaneous aggregation and its inhibition. (A) Aggregation kinetics of 11 μM HTT exon-Q_{23} alone (■) and in the presence of 18 μM of HTT^{NT} (□), 13 μM $HTT^{NT}Q_{23}P_{10}K_2$ alone (red filled circle) and in the presence of 18 μM of HTT^{NT} (red open circle), 18 μM HTT^{NT} alone (blue triangle), 40 μM $K_2Q_{23}K_2$ (green star), and 4 μM $HTT^{NT}Q_{23}K_2$ (green square). (B) Aggregation kinetics of 5.5 μM HTT exon1-Q_{42} alone (■) and in the presence of 9.1 μM of HTT^{NT} (□), 6.2 μM $HTT^{NT}Q_{42}P_{10}K_2$ alone (red filled circle) and in the presence of 9.1 μM of HTT^{NT} (red open circle), 9.1 μM HTT^{NT} alone (blue triangle), and 4.8 μM $K_2Q_{42}K_2$ (green star). All data points include error bars based on two measurements, except for the simple polyQ (green star) data.

Similar results were obtained with the Q_{42} versions of these peptides. The simple polyQ peptide $K_2Q_{42}K_2$ aggregates relatively slowly at 4.8 μM (Figure 3B, green star; note different time scale compared with panel A). Although we did not examine a $HTT^{NT}Q_{42}K_2$ molecule, we previously reported that the peptide $HTT^{NT}Q_{35}K_2$ aggregates to completion at 5 μM within about 3 h.[10] In analogy to the Q_{23} series, addition of a P_{10} sequence to generate $HTT^{NT}Q_{42}P_{10}K_2$ extends the aggregation time course so that a 6.2 μM reaction nears completion at about 70 h (Figure 3B, red filled circle). The aggregation of a 5.5 μM solution of full-length HTT exon1-Q_{42} (■) is somewhat slower than that of $HTT^{NT}Q_{42}P_{10}K_2$, but their relationship is qualitatively similar to the Q_{23} series, in that both Q_{42} versions of HTT exon1 aggregate faster than $K_2Q_{42}K_2$ and more slowly than $HTT^{NT}Q_{35}K_2$. Interestingly, there are

dx.doi.org/10.1021/bi500300c | Biochemistry 2014, 53, 3897−3907

some quantitative differences between the Q_{23} and Q_{42} series. First, the overall impact of the N- and C-terminal flanking sequences on aggregation appears to be greater for Q_{23} than for Q_{42}. This seems to be less due to the impact of the HTT^{NT} sequence, which is strong for both polyQ repeat lengths, and more due to the ability of PRD sequences to work against the rate enhancement by HTT^{NT}. Second, the presence of the full PRD sequence, in comparison to only a P_{10} sequence, has a measurable impact on Q_{42} kinetics but not Q_{23} kinetics. This effect might be due to reductions in non-β oligomer (Figure 2b,c,d) stability, in the efficiency of nucleation within this oligomer (Figure 2e), or in nucleus or fibril elongation (Figure 2f). As suggested by Figure 2, the preferred aggregation mechanism of HTT exon1-like peptides involves the initial formation of oligomeric intermediates, which have been demonstrated *in vitro* from incubation of both recombinant full-length HTT exon1[41] and chemically synthesized versions lacking full-length PRDs.[10]

Electron microscopy examination of early assembly intermediates of chemically synthesized, full-length HTT exon1-Q_{23} shows the existence of spherical oligomers (Figure 4D) and

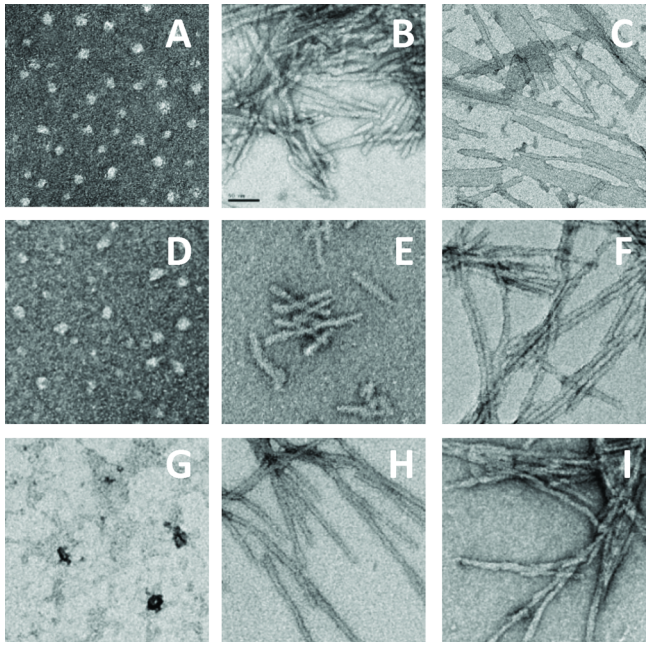

Figure 4. Negative stained electron micrographs of polyQ peptide aggregates. $HTT^{NT}Q_{23}P_{10}K_2$ at 7 h (10.5 ± 2.1 nm and 19.2 ± 1.4 nm) (A); $HTT^{NT}Q_{23}P_{10}K_2$ at 1000 h (12.0 ± 1.1 nm) (B); $K_2Q_{23}K_2$ at 300 h (C); HTT exon1-Q_{23} at 5 h (14.0 ± 2.3 and 24.0 ± 3.4 nm) (D); HTT exon1-Q_{23} at 30 h (17.2 ± 2.5 nm) (E); HTT exon1-Q_{23} at 1000 h (12.5 ± 1.5 nm) (F); HTT exon1-Q_{42} at 10 min (G); HTT exon1-Q_{42} 10 h (10.7 ± 1.5 nm) (H); and HTT exon1-Q_{42} at 70 h (11.5 ± 1.4 nm) (I). Scale bar = 50 nm. Diameters and standard deviations (parentheses) were obtained from 11 measurements using NIH ImageJ software. In two cases (images A and D) oligomers exhibited a broader size range and were analyzed as two components.

protofibril or fibril-like structures (Figure 4E) very similar in size and appearance to those described previously for the initial stages of the aggregation of an $HTT^{NT}Q_{30}P_6K_2$ peptide.[10] Nonamyloid (ThT-negative) oligomer formation has also been observed previously in the initial stages of $HTT^{NT}Q_{20}P_{10}K_2$ aggregation.[10] For a more direct comparison, we show here that spherical oligomers are also formed in the early hours of incubation of $HTT^{NT}Q_{23}P_{10}K_2$ (Figure 4A). Nonamyloid oligomers are also present in early incubation time points of HTT exon1-Q_{42} incubation (Figure 4G). Interestingly, the HTT exon1-Q_{42} oligomers exhibit qualitatively different staining properties in the EM. Despite this staining difference, we believe the oligomers formed early by both polyQ repeat length versions of full-length HTT exon1 are structurally similar, because both aggregation reactions exhibit similar sensitivities to inhibition by HTT^{NT} peptides (Figure 2; see below).

Dynamic light scattering (DLS) analysis of early time points of these incubation reactions are shown in Figure 5. The DLS

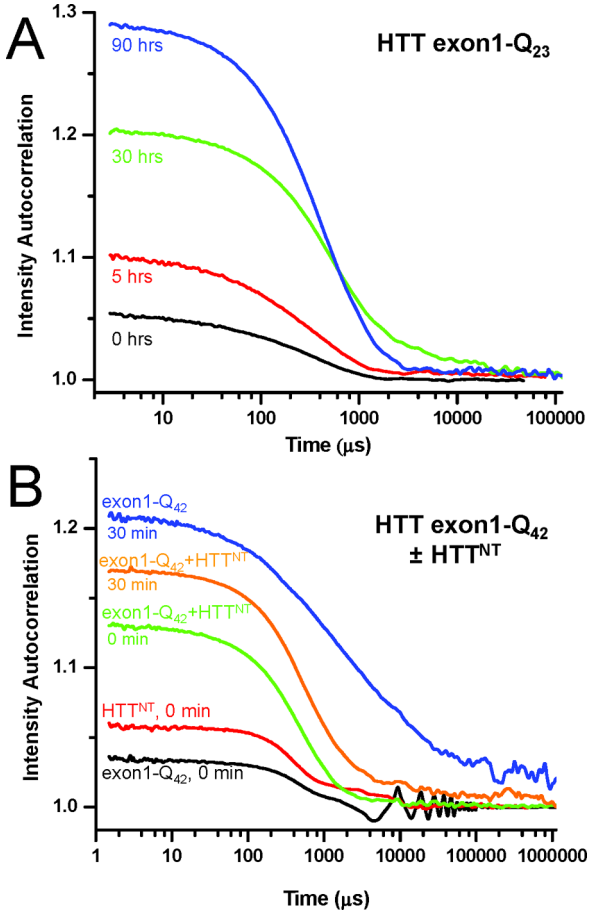

Figure 5. Analysis of aggregation by dynamic light scattering. Particle sizes from the DLS curves are listed in parentheses, as hydrodynamic radii. (A) Intensity correlation of 12 μM HTT exon1-Q_{23} at different times: 0 h (1.2 nm); 5 h (2.6 nm); 30 h (80 nm); and 90 h (98 nm). (B) Intensity correlation of 5.2 μM HTT exon1-Q_{42} alone at 0 h (identical to buffer alone; not shown) and 30 min (no correlation); 5.2 μM HTT exon1Q_{42} with 10.7 μM HTT^{NT} at 0 h (~8 nm) and 30 min (~8–10 nm); 10.7 μM HTT^{NT} at 0 h (identical to buffer alone; not shown).

curves of aliquots of the reaction mixtures at t = 0 exhibit amplitudes in the range of 1.05 or less and are indistinguishable from PBS buffer (not shown). The DLS time courses give particle size progressions as expected from the EM analysis, with rough agreement in absolute values at different time points. Thus, for HTT exon1-Q_{23} at 5 h, EM shows a range of particle sizes centered at 14 and 24 nm in diameter (Figure 4 legend), while at the same time point DLS gives a homogeneous suspension of particles with ~5 nm diameter

dx.doi.org/10.1021/bi500300c | *Biochemistry* 2014, 53, 3897–3907

(2.6 nm hydrodynamic radius). At 30 h, EM shows a uniform population of protofibrils of ~17 nm in diameter and 50−130 nm in length, while DLS gives a hydrodynamic radius of 80 nm for a filament length in the 100−200 nm range, in good agreement with the EM analysis. HTT exon1-Q_{42} incubated for only 30 min yields scatter from a diverse population of particles that cannot be easily fit by the software (Figure 5B). This is typical of amyloid assembly reactions, in which time points associated with amyloid fibrils give strong scattering in DLS that fails to give an interpretable correlation.

Recently we described the ability of isolated HTT^{NT} peptides to act as inhibitors of the nucleation phase of the amyloid formation of HTT exon1-like peptides.[48] This ability appears to be due to the coassembly of the HTT^{NT} peptides with HTT exon1 during oligomer formation, by virtue of mixed helical bundle formation as shown in Figure 2i. This dilutes the average local concentration of polyQ chains within the mixed oligomers, reducing nucleation efficiency. Once nucleation occurs, however, amyloid formation proceeds unabated.[48] Since we found that HTT^{NT} in trans has no effect on simple polyQ aggregation,[48] we can use the sensitivity of an aggregation reaction to HTT^{NT} inhibition as a test of mechanism.

In fact, we found that, to different extents, both of the chemically synthesized, full-length HTT exon1 peptides used in this study are susceptible to HTT^{NT} inhibition (Figure 3). HTT exon1-Q_{23} is especially susceptible, showing only about 10% aggregation in the presence of a 1.5-fold molar excess of HTT^{NT} (□) at 1000 h, a time when the peptide without inhibitor has essentially aggregated to completion (Figure 3A, ■). Mirroring their overlapping aggregation curves, $HTT^{NT}Q_{23}P_{10}K_2$ exhibits inhibition kinetics (red open circle) very similar to the inhibition of HTT exon1-Q_{23} (Figure 3A, □). HTT^{NT} inhibition of Q_{42} HTT exon1-like peptides is somewhat less effective than for the Q_{23} peptides. At a time when the uninhibited reaction of $HTT^{NT}Q_{42}P_{10}K_2$ (red filled circle) is 50% aggregated (about 11 h), it is about 30% aggregated in the presence of a ~1.5-fold molar excess of HTT^{NT} (Figure 3B, red open circle). Full-length HTT exon1-Q_{42} is more susceptible to inhibition, so in the presence of 1.5-fold HTT^{NT} it has aggregated only negligibly at 25 h (Figure 3B, □), when the uninhibited reaction is 50% aggregated (Figure 3B, ■). Consistent with the proposed mechanism of HTT^{NT} inhibition involving coassembly, the $t = 0$ time point of a mixture of HTT^{NT} plus HTT exon1-Q_{42} exhibits more scattering intensity than the $t = 0$ time point of either component alone (Figure 5B). At the same time, oligomer size grows modestly within the lag phase of the inhibited reaction, giving an interpretable DLS curve after 30 min incubation (Figure 5B), consistent with a buildup of larger, HTT^{NT}-mediated oligomers. As noted above, the same amount of HTT exon1-Q_{42} incubated without HTT^{NT} for the same time gives more scattering and larger scattering particles (Figure 5B). As noted above, the sensitivity of HTT exon1-Q_{42} aggregation to inhibition by HTT^{NT} peptides suggests that, as shown for other HTT exon1 analogues,[48] the amyloid nucleation pathway must involve a required intermediate featuring HTT^{NT}-based, nonamyloid assembly. That is, this pathological repeat length HTT exon1 must undergo amyloid nucleation via the A pathway shown in Figure 2.

Aggregate Structure. We assessed the impact of the PRD on polyQ amyloid structure by electron microscopy, dynamic light scattering, FTIR, fibril stability measurements, and cross-seeding experiments. By EM, the mature fibrils produced by both the Q_{23} (Figure 4F) and Q_{42} (Figure 4I) versions of chemically synthesized full-length HTT exon1 exhibit similar morphologies, both to each other and to fibrils from both chemically synthesized model peptides of the $HTT^{NT}Q_NP_{10}K_2$ design (Figure 4B)[44] and from recombinantly produced, nearly exact full-length HTT exon1 peptides.[39] One unexpected result is that at an intermediate time point in the aggregation of the chemically synthesized HTT exon1 peptides, the Q_{23} version, but not the Q_{42} version, exhibits a remarkably uniform population of very short fibrils with lengths in the 50−130 nm range (Figure 4E). Interestingly, these particles have somewhat larger diameters than mature fibrils in the EM, on the order of 17.2 nm compared with the fibril diameter of 12.5 nm (Figure 4). It is possible that these structures are related to the protofibrils often observed at intermediate times in the assembly of other amyloids. As in the case of these other amyloids, the role of the structures shown in Figure 4E in the assembly of mature amyloid fibrils is not clear. As observed previously,[15] the mature fibrils of polyQ peptides containing HTT flanking sequences are substantially different in EM morphology from the amyloid produced by simple polyQ peptides (Figure 4C).

The size distribution of HTT exon1 aggregation products is of some interest, because of ongoing efforts to identify the toxic molecular species that is presumably populated in a time- and repeat length-dependent manner in the pathogenic mechanism of HD.[9] In particular, it has become important to gauge the size range of aggregates in the context of the limited ability of fluorescence microscopy to detect aggregates smaller than inclusions (see Discussion). We therefore calculated the number of HTT exon1 monomers that could be packed into some of the smaller aggregates we observed from incubation of HTT exon1-Q_{23}, using an estimate for the density of a folded protein of 1.37 g/cm^3.[57] For the spherical oligomers observed at 5 h by EM (Figure 4D), we calculated that the oligomers contain from 123 to 623 molecules, while the short fibrils or protofibrils observed at 30 h (Figure 3E) contain from 530 to 2740 molecules.

Despite the EM differences between HTT exon1 fibrils and simple polyQ fibrils, there is substantial evidence that the polyQ amyloid cores of these various aggregates are largely identical. For example, the second derivative FTIR spectra of the truncated and full-length HTT exon1 aggregates are essentially identical to the spectrum of a simple polyQ peptide amyloid (Figure 6). In particular, the three bands characteristic of simple polyQ amyloid [1605 cm^{-1} (glutamine side chain N−H bending), 1625 cm^{-1} (β-sheet), and 1659 cm^{-1} (glutamine side chain C=O stretch)] dominate all of the amyloid fibrils derived from HTT exon1-related peptides. In addition, both for Q_{23} and for Q_{42} versions, the FTIR spectra of the full HTT exon1 and $HTT^{NT}Q_NP_{10}K_2$ aggregates are superimposable (Figure 6). The small differences that exist between spectra, located in the broad region from 1610 to 1640 cm^{-1} that is normally associated with β-structure,[58] recur in other FTIR spectra of polyQ aggregates[11,56] without correlating with any obvious primary sequence feature, be it polyQ repeat length or the presence or absence of flanking sequences. We think it is likely that the fine structure sometimes observed in this region, as seen in the spectra for the Q_{23} peptide aggregates in Figure 6, is related to better signal in these spectra due to the availability of larger amounts of sample.

A powerful measure of the relatedness of two amyloid systems is the ability of the fibrils of one to "cross-seed" the

dx.doi.org/10.1021/bi500300c | Biochemistry 2014, 53, 3897−3907

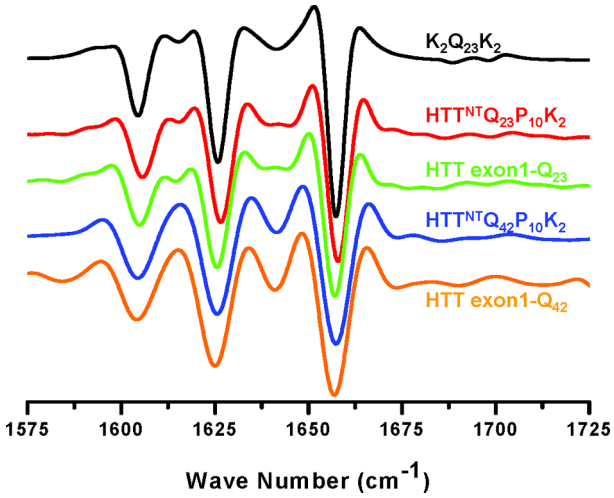

Figure 6. FTIR spectra of isolated final aggregates. The second derivative spectra of aggregates collected, when the aggregation reaction was judged complete, at the following times: $K_2Q_{23}K_2$ (300 h); $HTT^{NT}Q_{23}P_{10}K_2$ (1000 h); HTT exon1-Q_{23} (1000 h); $HTT^{NT}Q_{42}P_{10}K_2$ (70 h); and HTT exon1-Q_{42} (70 h).

elongation of monomers of the other.[59] In general, the efficiency of seeding elongation is thought to depend on the structural compatibility between the monomer and the fibril seed. We found excellent "cross-talk" between fibrils of $HTT^{NT}Q_{23}P_{10}K_2$ and HTT exon1-Q_{23}. Thus, in an experiment with equal concentrations of freshly disaggregated HTT exon1-Q_{23} monomers, the addition of 20% by weight of amyloid fibrils gives essentially the same enhanced aggregation kinetics for seeds of either HTT exon1-Q_{23} (red filled circle) and $HTT^{NT}Q_{23}P_{10}K_2$ (blue triangle) amyloid, when compared with the spontaneous, unseeded aggregation reaction (■) (Figure 7A). Similarly, with freshly disaggregated $HTT^{NT}Q_{23}P_{10}K_2$ monomers, 20% by weight of $HTT^{NT}Q_{23}P_{10}K_2$ amyloid (red filled circle) and HTT exon1-Q_{23} amyloid (blue triangle) gives identical aggregation stimulation compared with monomer alone (Figure 7B, ■). We take this to indicate a strong similarity in the polyQ amyloid cores of these two peptide fibrils.

Another method for characterizing amyloid structures is by the stabilities of the fibrils against dissociation.[60] Unless the monomers within a fibril are chemically cross-linked, fibrils should generally be capable of dissociating to monomers in native buffer until an equilibrium position is reached,[60] and this position is a measure of fibril stability with values that can be quite robust.[61] Fibril stabilities as estimated by C_r determinations were previously successfully used to conduct several comparative studies of amyloid stability, including a set of polymorphic amyloid fibrils derived from the same Aβ_{40} sequence,[62] fibrils generated from simple polyQ of different repeat lengths,[31] and fibrils generated from polyQ molecules with or without β-hairpin encouraging mutations.[63] Here we determined the equilibrium positions, expressed as the concentration of monomer at equilibrium (the C_r value), for various Q_{23} versions of HTT exon1 and compared the results with the previously published[56] value for $K_2Q_{23}K_2$. When HTT exon1-Q_{23} is incubated at ~9 μM, it aggregates slowly over a period of weeks, reaching an equilibrium concentration of monomer after about one month (Figure 8A, ■). When this final aggregation reaction is diluted to reduce the concentration of monomer and the diluted reaction is further incubated, the

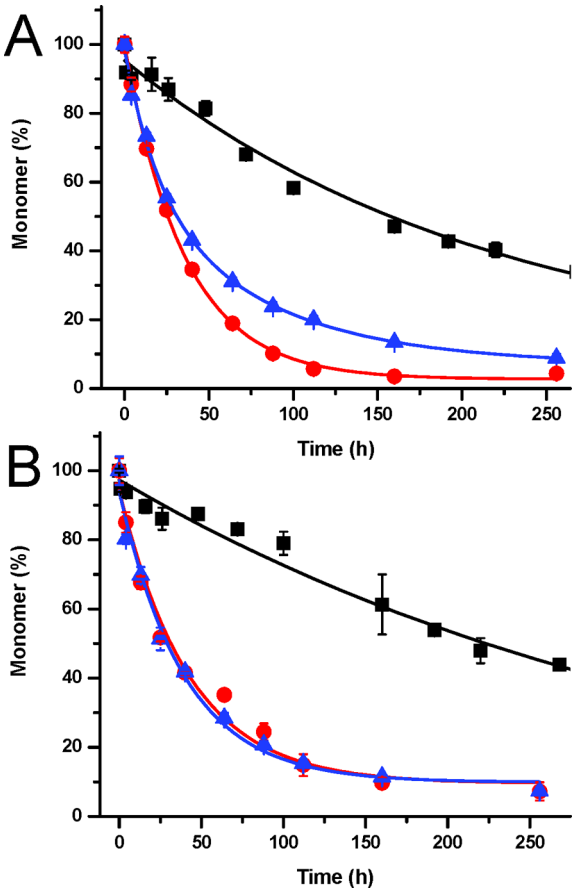

Figure 7. Seeded aggregation kinetics. Monomer alone (■), self-seeding (red filled circle), and cross-seeding (blue triangle): (A) 11 μM HTT exon1-Q_{23} monomer alone (■) or seeded with 20% by weight of amyloid fibrils of either HTT exon1-Q_{23} (red filled circle) or $HTT^{NT}Q_{23}P_{10}K_2$ (blue triangle); (B) 13 μM $Htt^{NT}Q_{23}P_{10}K_2$ monomer alone (■) or seeded with 20% by weight of amyloid fibrils of either $HTT^{NT}Q_{23}P_{10}K_2$ (red filled circle) or HTT exon1-Q_{23} (blue triangle). All data points have error bars based on two measurements.

monomer concentration increases as fibrils dissociate (red square), until equilibrium is reestablished, also after a period of about one month (Figure 8A, inset). The mean of the equilibrium positions measured for the association and dissociation directions for this peptide is 0.44 ± 0.13 μM. This C_r value, the concentration of monomer below which aggregation is thermodynamically disallowed, is a convenient measure of fibril stability; the lower C_r, the more stable the fibril. A similar analysis of $HTT^{NT}Q_{23}P_{10}K_2$ (Figure 8B) gives a C_r value of 0.28 ± 0.11. Thus, fibrils of full-length HTT exon1 and of the C-terminally truncated version are of essentially equal stability. Unfortunately, we could not obtain the corresponding values for the Q_{42} peptides, since these appear to be below our level of detection.

We obtained two additional C_r values. Previously we reported a value of 3.0 μM for the C_r of $K_2Q_{23}K_2$ amyloid.[56] In the present study, we determined a C_r of ≤0.1 μM for $HTT^{NT}Q_{23}K_2$ (the actual value may be lower, but the limited sensitivity of our methods preclude measuring concentrations below 0.1 μM for these peptides). These C_r values allow us to calculate a number of important $\Delta\Delta G$ values or limits. By comparing the values for $K_2Q_{23}K_2$ and $HTT^{NT}Q_{23}K_2$, we obtain a positive contribution of the HTT^{NT} sequence to amyloid stability of ≥2.2 kcal/mol. This is consistent with previous data,

dx.doi.org/10.1021/bi500300c | *Biochemistry* 2014, 53, 3897−3907

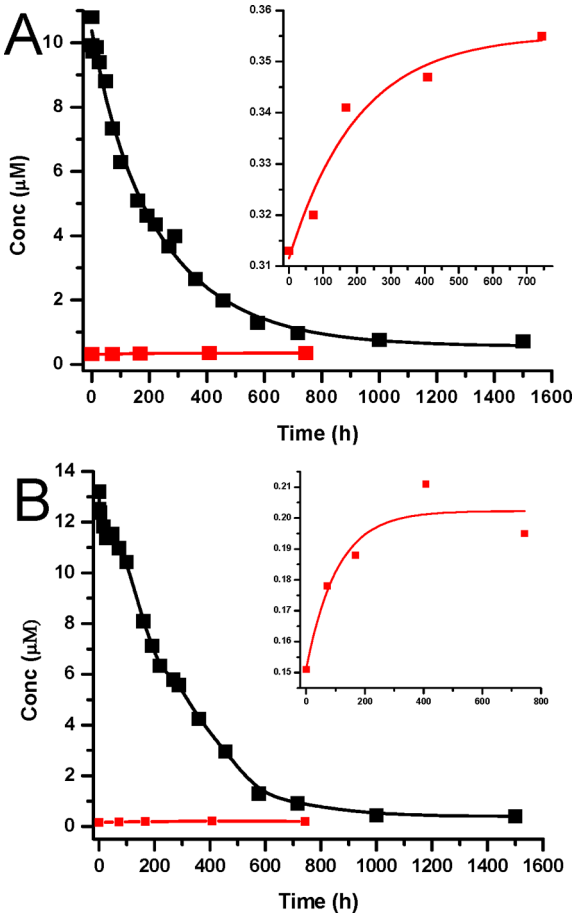

Figure 8. Determination of the equilibrium position of amyloid assembly and disassembly. Spontaneous aggregation (■) and dissociation (red square) of amyloid fibrils of HTT exon1-Q_{23} (A; $C_r = 0.44 \pm 0.13$ μM) and $HTT^{NT}Q_{23}P_{10}K_2$ (B; $C_r = 0.28 \pm 0.11$ μM). Insets, dissociation shown on expanded *y*-axis.

suggesting that HTT^{NT} remains α-helical in assembled fibrils and appears to self-associate in that context.[11,45,64] By comparing the limit found for $HTT^{NT}Q_{23}K_2$ with the value of C_r found for HTT exon1-Q_{23}, we can conclude that the PRD of HTT exon1 destabilizes amyloid fibrils by ≥0.9 kcal/mol. This is consistent with previous results on the effect of a short polyPro sequence on polyQ amyloid stability.[65]

DISCUSSION

In this paper, we provide data showing that chemically synthesized HTT exon1 peptides, containing precise Met-Ala-Thr N-terminal starts and containing a complete C-terminus without any sequence tag extensions, self-associate with very similar kinetics and aggregate morphologies to HTT exon1 analogues containing only the P_{10} sequence. We observed slightly slower aggregation kinetics in the Q_{42} background for full HTT exon1 compared with the P_{10} version. The structures of the mature amyloid fibrils, the presence of oligomeric intermediates in electron micrographs at early incubation times, and the sensitivity to HTT^{NT} inhibition of aggregation strongly suggest that these full-length HTT exon1 analogues aggregate by the same two-step mechanism deduced for C-terminally truncated HTT exon1 peptides.[10]

If some kind of self-assembled, aggregated state of HTT exon1 is responsible for triggering HD, a drug discovery paradigm that cannot be neglected is the search for inhibitors that prevent or slow this process. Previously we showed that peptide-based inhibitors structurally related to the HTT^{NT} segment are effective agents for delaying the nucleation of amyloid formation by HTT exon1 analogues with truncated C-termini.[48] We show here that HTT^{NT} is equally or more effective at delaying nucleation in the chemically synthesized full-length HTT exon1 peptides. In the case of the Q_{42} repeat length HTT exon1, the onset of amyloid formation is delayed by about 2 days compared with the uninhibited reaction. Even short delays of nucleation may be effective in suppressing the buildup of toxic aggregates, since theoretically it would allow time for other cellular processes to remove aggregation-prone precursors.

Within the resolution of the FTIR technique, the polyQ amyloid cores of all the polyQ peptides tested are remarkably similar, suggesting that, despite differences in the mechanisms of assembly and mature amyloid morphology, the underlying cross-β structure of the polyQ amyloid is similar. At the same time, the presence of flanking sequences can have profound effects, not only on fibril morphology but also on fibril stability. The presence of HTT^{NT} contributes over 2 kcal/mol to the stability of the fibrils toward dissociation, while, in contrast, the addition of some form of PRD reduces stability by 1 kcal/mol or more. The exact nature of the PRD appears to make a negligible difference in this stability effect, with the P_{10} sequence being sufficient to represent essentially the full fibril destabilizing action of the PRD.

One interesting aspect of the C_r measurement that generated the above stability values is the dissociation kinetics of HTT exon1 amyloid. Previously we reported very slow dissociation kinetics for simple polyQ amyloid fibrils, with $K_2Q_{23}K_2$ fibrils requiring about 2 months to dissociate to equilibrium.[56] We show here that HTT exon1 analogues feature a similarly slow dissociation rate, despite the presence of flanking sequences that modulate the thermodynamic stability of the fibrils. Thus, while $A\beta_{40}$ amyloid dissociates to equilibrium in PBS at 37 °C over a period of only 24 h,[60] it takes about 4 weeks for HTT exon1-Q_{23} (or $HTT^{NT}Q_{23}P_{10}K_2$) fibrils to dissociate to equilibrium (Figure 8). These new data suggest that the slow kinetics are relatively unaffected by flanking sequences and therefore are likely be tied to the structure of the polyQ amyloid core. Interestingly, aggregates of an HTT exon1-Q_{94} protein expressed in the brains of a mouse model required 3 weeks to dissociate after HTT exon1 expression was turned off.[66] The authors reported data supporting a role of the ubiquitin proteasome system in the clearance of these aggregates (as well as monomers).[66] Together with those findings, our data are consistent with the hypothesis that the dissociation rate of aggregates in the mouse brain is driven primarily by the biophysical properties of the HTT exon1 amyloid and not by cellular factors. The role of the proteasome may be simply to help remove monomeric HTT exon1 from the thermodynamic system, which would tend to drive dissolution by virtue of Le Chatelier's principle.

One issue that continues to plague the HD field is our ignorance of the potential size range of aggregated proteins in the cell. Although evidence has been presented that the large inclusions observed in HD cells and cell models are more likely to be protective than toxic,[33] these data have no bearing on a possible role for any smaller aggregated species that might exist in the cell.[67] In fact, the inclusions easily observed in HD brain tissue and cell models tend to be about 5 μm in diameter,

dx.doi.org/10.1021/bi500300c | *Biochemistry* 2014, 53, 3897−3907

corresponding roughly to an HTT exon1 content of 10^9 molecules,[9] and this allows for a huge range of smaller aggregate sizes that will presumably be more difficult to detect in cells or cell extracts. In fact, super-resolution fluorescence microscopy was recently used to detect individual amyloid fibrils in a cell model of HD.[34] We calculate these fibrils to have monomer contents in the range of 10^5 monomers per aggregate.[9] In the present paper, we show that well-characterized full-length HTT exon1 peptides aggregated *in vitro* are capable of populating even smaller aggregates during amyloid assembly: spherical oligomers with monomer contents in the range of 100−600 and short, linear, protofibril-like structures with monomer contents in the range of 500−2600. These are in addition to much longer amyloid fibrils that develop later in aggregation reactions. While our data do not prove that such small aggregates exist or accumulate in the cell, it is clear that these aggregates have sufficient kinetics of formation and stabilities *in vitro* that their formation in cells is energetically feasible.

It is interesting to put these findings in the context of results of other studies. EM-characterized aggregates of similar sizes, much smaller than inclusions but much larger than monomer, have been generated either by *in vitro* incubation of recombinantly produced HTT exon1[41] or by isolation from brain homogenates of a HD mouse model.[68] A variety of aggregate sizes has been revealed by analysis of lysates of cell or tissue from HD models or HD patients, which, in order of increasing estimated number of peptide monomers per aggregate, are 4-mers (B. Sahoo et al., msc submitted), 5-mers to 15-mers,[36] ∼10-mers (assuming a composition of HTT exon1-sized proteolytic fragments),[38] 200-mers,[42] and 50−10000-mers (B. Sahoo et al., msc submitted).

Recombinant DNA methods of synthesizing useful amounts of peptides and proteins[69] have revolutionized protein biochemistry and biophysics research, oftentimes making studies possible that otherwise simply could not be undertaken. The HTT exon1 peptide lies at an intermediate size range, which, ironically, provides different but equally significant challenges for both recombinant and chemical synthesis, perhaps in particular in conducting aggregation studies. While this peptide is somewhat longer than the typical upper limit to solid phase synthesis, it is too small and aggregation prone for successful cell production unless it is fused with a partner that limits its aggregation. This fusion partner must then be removed chemically or proteolytically *in vitro*.

For peptides with lengths within the synthesis limits, chemical synthesis can deliver precisely designed molecules. However, in addition to the size limit, chemical synthesis can generate difficult-to-remove peptide side products and other impurities,[55] including D-amino acids from epimerization during synthesis that can be very difficult to detect but that, even in small amounts, can compromise amyloid formation.[70] Recombinant synthesis, in contrast, can generate peptides and proteins of much greater length with relative ease and initially high sequence fidelity. However, it appears that the properties of the same sequence produced in different cell types can sometimes differ considerably, presumably due to variations in post-translational modifications.[43] Furthermore, exigencies of cloning or proteolytic release of desired peptides from fusion partners can sometimes lead to small but potentially significant modifications in the recombinant product, such as in extensions[42,71,72] or truncations[71] of the HTT^{NT} sequence. If the modifications occur in a portion of the molecule that is critical to its solution properties, the seemingly small compromises made to produce the recombinant peptide could have unintended consequences. For example, the use of trypsin as one option for cleaving HTT exon1 from an N-terminal fusion partner[71] almost certainly leads to cleavage at one or more of the lysine residues within HTT^{NT}.[10] This appears to generate an amyloid fibril morphology[71] that more resembles the ribbon-like aggregates produced from simple polyQ peptides[46] (Figure 4C) than the isolated filaments produced from HTT exon1-like peptides with intact N-termini (Figure 4F,I). In situations such as that presented by HTT exon1, it will continue to be important to investigate the possible impact of the effects of these compromises on experimental results.

Chemically accessible, C-terminally truncated versions of HTT exon1 and related molecules have been utilized to deduce the mechanism of the aggregation enhancing effect of the HTT^{NT} N-terminal segment of HTT,[10,11,46−48] assess the impact of serine phosphorylation within HTT^{NT} on that mechanism,[44,47] characterize the magnitude and nature of the polyproline effect on aggregation,[10,50,65] determine aspects of HTT exon1 amyloid structure,[45] characterize aggregation inhibition by HTT^{NT} peptides,[48] and monitor HTT exon1−membrane interactions.[49] The recent availability of chemically synthesized, full-length HTT exon1 peptides[53,73] has offered the possibility that, given sufficient yields of pure material, systematic *in vitro* studies can now be conducted on molecules more accurately resembling the HTT exon1 fragments generated in the cell. In this paper, we describe in detail characterization of the aggregation properties of such chemically synthesized full-length HTT exon1 containing both benign and pathological polyQ repeat lengths. Our data show that the PRD of HTT exon1 beyond the first 10 prolines contributes only modest quantitative differences in some biophysical properties, while other properties seem to be essentially unchanged. The data suggest that these truncated molecules can be valuable substitutes for full-length HTT exon1 when chemically precise versions of the latter are not available.

AUTHOR INFORMATION

Corresponding Author

*E-mail: rwetzel@pitt.edu. Phone: 412-383-5271.

Funding

We gratefully acknowledge funding support from the National Institutes of Health (Grant AG019322 to R.W.) and the German Federal Ministry of Education and Research (BMBF) (Go-Bio Project 0315988 to T.Z.).

Notes

The authors declare no competing financial interest.

ACKNOWLEDGMENTS

EMs were collected in the University of Pittsburgh School of Medicine's Structural Biology Department EM facility administered by Drs. James Conway and Alexander Makhov.

REFERENCES

(1) Bates, G., Harper, P. S., and Jones, L., Eds. (2002) *Huntington's Disease*, 3rd ed., Oxford University Press, Oxford, U.K.

(2) Bates, G., Tabrizi, S. J., and Jones, L., Eds. (2014) *Huntington's Disease*, 4th ed., Oxford University Press, Oxford, U.K.

(3) Bates, G. P., and Benn, C. (2002) The polyglutamine diseases, In *Huntington's Disease* (Bates, G. P., Harper, P. S., and Jones, L., Eds.), pp 429−472, Oxford University Press, Oxford, U.K.
(4) Wilburn, B., Rudnicki, D. D., Zhao, J., Weitz, T. M., Cheng, Y., Gu, X. F., Greiner, E., Park, C. S., Wang, N., Sopher, B. L., La Spada, A. R., Osmand, A., Margolis, R. L., Sun, Y. E., and Yang, X. W. (2011) An antisense CAG repeat transcript at JPH3 locus mediates expanded polyglutamine protein toxicity in Huntington's disease-like 2 mice. *Neuron 70*, 427−440.
(5) Landles, C., Sathasivam, K., Weiss, A., Woodman, B., Moffitt, H., Finkbeiner, S., Sun, B., Gafni, J., Ellerby, L. M., Trottier, Y., Richards, W. G., Osmand, A., Paganetti, P., and Bates, G. P. (2010) Proteolysis of mutant huntingtin produces an exon 1 fragment that accumulates as an aggregated protein in neuronal nuclei in Huntington disease. *J. Biol. Chem. 285*, 8808−8823.
(6) Sathasivam, K., Neueder, A., Gipson, T. A., Landles, C., Benjamin, A. C., Bondulich, M. K., Smith, D. L., Faull, R. L., Roos, R. A., Howland, D., Detloff, P. J., Housman, D. E., and Bates, G. P. (2013) Aberrant splicing of HTT generates the pathogenic exon 1 protein in Huntington disease. *Proc. Natl. Acad. Sci. U. S. A. 110*, 2366−2370.
(7) Bates, G. P., Mangiarini, L., Mahal, A., and Davies, S. W. (1997) Transgenic models of Huntington's disease. *Hum. Mol. Genet. 6*, 1633−1637.
(8) Dyson, H. J., and Wright, P. E. (2005) Intrinsically unstructured proteins and their functions. *Nat. Rev. Mol. Cell Biol. 6*, 197−208.
(9) Wetzel, R., and Mishra, R. (2014) Structural biology: Order, disorder, and conformational flux, In *Huntington's Disease* (Bates, G., Tabrizi, S. J., and Jones, L., Eds.), pp 274−322, Oxford University Press, Oxford, U.K.
(10) Thakur, A. K., Jayaraman, M., Mishra, R., Thakur, M., Chellgren, V. M., Byeon, I. J., Anjum, D. H., Kodali, R., Creamer, T. P., Conway, J. F., Gronenborn, A. M., and Wetzel, R. (2009) Polyglutamine disruption of the huntingtin exon 1 N terminus triggers a complex aggregation mechanism. *Nat. Struct. Mol. Biol. 16*, 380−389.
(11) Jayaraman, M., Kodali, R., Sahoo, B., Thakur, A. K., Mayasundari, A., Mishra, R., Peterson, C. B., and Wetzel, R. (2012) Slow amyloid nucleation via alpha-helix-rich oligomeric intermediates in short polyglutamine-containing huntingtin fragments. *J. Mol. Biol. 415*, 881−899.
(12) Michalek, M., Salnikov, E. S., Werten, S., and Bechinger, B. (2013) Membrane Interactions of the Amphipathic Amino Terminus of Huntingtin. *Biochemistry 52*, 847−858.
(13) Chen, S., Berthelier, V., Yang, W., and Wetzel, R. (2001) Polyglutamine aggregation behavior in vitro supports a recruitment mechanism of cytotoxicity. *J. Mol. Biol. 311*, 173−182.
(14) Crick, S. L., Jayaraman, M., Frieden, C., Wetzel, R., and Pappu, R. V. (2006) Fluorescence correlation spectroscopy shows that monomeric polyglutamine molecules form collapsed structures in aqueous solutions. *Proc. Natl. Acad. Sci. U. S. A. 103*, 16764−16769.
(15) Wetzel, R. (2012) Physical chemistry of polyglutamine: Intriguing tales of a monotonous sequence. *J. Mol. Biol. 421*, 466−490.
(16) Wang, X., Vitalis, A., Wyczalkowski, M. A., and Pappu, R. V. (2006) Characterizing the conformational ensemble of monomeric polyglutamine. *Proteins 63*, 297−311.
(17) Dlugosz, M., and Trylska, J. (2011) Secondary Structures of Native and Pathogenic Huntingtin N-Terminal Fragments. *J. Phys. Chem. B 115*, 11597−11608.
(18) Caron, N. S., Desmond, C. R., Xia, J. R., and Truant, R. (2013) Polyglutamine domain flexibility mediates the proximity between flanking sequences in huntingtin. *Proc. Natl. Acad. Sci. U.S.A. 110*, 14610−14615.
(19) Miller, J., Arrasate, M., Brooks, E., Libeu, C. P., Legleiter, J., Hatters, D., Curtis, J., Cheung, K., Krishnan, P., Mitra, S., Widjaja, K., Shaby, B. A., Lotz, G. P., Newhouse, Y., Mitchell, E. J., Osmand, A., Gray, M., Thulasiramin, V., Saudou, F., Segal, M., Yang, X. W., Masliah, E., Thompson, L. M., Muchowski, P. J., Weisgraber, K. H., and Finkbeiner, S. (2011) Identifying polyglutamine protein species in situ that best predict neurodegeneration. *Nat. Chem. Biol. 7*, 925−934.
(20) Peters-Libeu, C., Miller, J., Rutenber, E., Newhouse, Y., Krishnan, P., Cheung, K., Hatters, D., Brooks, E., Widjaja, K., Tran, T., Mitra, S., Arrasate, M., Mosquera, L. A., Taylor, D., Weisgraber, K. H., and Finkbeiner, S. (2012) Disease-associated polyglutamine stretches in monomeric huntingtin adopt a compact structure. *J. Mol. Biol. 421*, 587−600.
(21) Buchanan, L. E., Carr, J. K., Fluitt, A. M., Hoganson, A. J., Moran, S. D., de Pablo, J. J., Skinner, J. L., and Zanni, M. T. (2014) Structural motif of polyglutamine amyloid fibrils discerned with mixed-isotope infrared spectroscopy. *Proc. Natl. Acad. Sci. U. S. A. 111*, 5796−5801.
(22) Bennett, M. J., Huey-Tubman, K. E., Herr, A. B., West, A. P., Ross, S. A., and Bjorkman, P. J. (2002) A linear lattice model for polyglutamine in CAG expansion diseases. *Proc. Natl. Acad. Sci. U. S. A. 99*, 11634−11639.
(23) Klein, F. A., Zeder-Lutz, G., Cousido-Siah, A., Mitschler, A., Katz, A., Eberling, P., Mandel, J. L., Podjarny, A., and Trottier, Y. (2013) Linear and extended: a common polyglutamine conformation recognized by the three antibodies MW1, 1C2 and 3B5H10. *Hum. Mol. Genet. 22*, 4215−4223.
(24) Bates, G. (2003) Huntingtin aggregation and toxicity in Huntington's disease. *Lancet 361*, 1642−1644.
(25) Ross, C. A., and Poirier, M. A. (2005) Opinion: What is the role of protein aggregation in neurodegeneration? *Nat. Rev. Mol. Cell Biol. 6*, 891−898.
(26) Michalik, A., and Van Broeckhoven, C. (2003) Pathogenesis of polyglutamine disorders: Aggregation revisited. *Hum. Mol. Genet. 12* (Suppl 2), R173−186.
(27) DiFiglia, M., Sapp, E., Chase, K. O., Davies, S. W., Bates, G. P., Vonsattel, J. P., and Aronin, N. (1997) Aggregation of huntingtin in neuronal intranuclear inclusions and dystrophic neurites in brain. *Science 277*, 1990−1993.
(28) Cooper, J. K., Schilling, G., Peters, M. F., Herring, W. J., Sharp, A. H., Kaminsky, Z., Masone, J., Khan, F. A., Delanoy, M., Borchelt, D. R., Dawson, V. L., Dawson, T. M., and Ross, C. A. (1998) Truncated N-terminal fragments of huntingtin with expanded glutamine repeats form nuclear and cytoplasmic aggregates in cell culture. *Hum. Mol. Genet. 7*, 783−790.
(29) Davies, S. W., Turmaine, M., Cozens, B. A., DiFiglia, M., Sharp, A. H., Ross, C. A., Scherzinger, E., Wanker, E. E., Mangiarini, L., and Bates, G. P. (1997) Formation of neuronal intranuclear inclusions underlies the neurological dysfunction in mice transgenic for the HD mutation. *Cell 90*, 537−548.
(30) Gusella, J. F., and MacDonald, M. E. (2000) Molecular genetics: Unmasking polyglutamine triggers in neurodegenerative disease. *Nat. Rev. Neurosci 1*, 109−115.
(31) Landrum, E., and Wetzel, R. (2014) Biophysical Underpinnings of the Repeat Length Dependence of Polyglutamine Amyloid Formation. *J. Biol. Chem. 289*, 10254−10260.
(32) Morley, J. F., Brignull, H. R., Weyers, J. J., and Morimoto, R. I. (2002) The threshold for polyglutamine-expansion protein aggregation and cellular toxicity is dynamic and influenced by aging in Caenorhabditis elegans. *Proc. Natl. Acad. Sci. U. S. A. 99*, 10417−10422.
(33) Arrasate, M., Mitra, S., Schweitzer, E. S., Segal, M. R., and Finkbeiner, S. (2004) Inclusion body formation reduces levels of mutant huntingtin and the risk of neuronal death. *Nature 431*, 805−810.
(34) Sahl, S. J., Weiss, L. E., Duim, W. C., Frydman, J., and Moerner, W. E. (2012) Cellular inclusion bodies of mutant huntingtin exon 1 obscure small fibrillar aggregate species. *Sci. Rep. 2*, 895.
(35) Luo, S., Mizuta, H., and Rubinsztein, D. C. (2008) p21-activated kinase 1 promotes soluble mutant huntingtin self-interaction and enhances toxicity. *Hum. Mol. Genet. 17*, 895−905.
(36) Ossato, G., Digman, M. A., Aiken, C., Lukacsovich, T., Marsh, J. L., and Gratton, E. (2010) A two-step path to inclusion formation of huntingtin peptides revealed by number and brightness analysis. *Biophys. J. 98*, 3078−3085.

(37) Lajoie, P., and Snapp, E. L. (2010) Formation and Toxicity of Soluble Polyglutamine Oligomers in Living Cells. *PLoS One 5*, No. e15245.
(38) Marcellin, D., Abramowski, D., Young, D., Richter, J., Weiss, A., Marcel, A., Maassen, J., Kauffmann, M., Bibel, M., Shimshek, D. R., Faull, R. L., Bates, G. P., Kuhn, R. R., Van der Putten, P. H., Schmid, P., and Lotz, G. P. (2012) Fragments of HdhQ150 mutant huntingtin form a soluble oligomer pool that declines with aggregate deposition upon aging. *PLoS One 7*, No. e44457.
(39) Scherzinger, E., Sittler, A., Schweiger, K., Heiser, V., Lurz, R., Hasenbank, R., Bates, G. P., Lehrach, H., and Wanker, E. E. (1999) Self-assembly of polyglutamine-containing huntingtin fragments into amyloid-like fibrils: implications for Huntington's disease pathology. *Proc. Natl. Acad. Sci. U. S. A. 96*, 4604−4609.
(40) Heiser, V., Scherzinger, E., Boeddrich, A., Nordhoff, E., Lurz, R., Schugardt, N., Lehrach, H., and Wanker, E. E. (2000) Inhibition of huntingtin fibrillogenesis by specific antibodies and small molecules: implications for Huntington's disease therapy. *Proc. Natl. Acad. Sci. U. S. A. 97*, 6739−6744.
(41) Poirier, M. A., Li, H., Macosko, J., Cai, S., Amzel, M., and Ross, C. A. (2002) Huntingtin spheroids and protofibrils as precursors in polyglutamine fibrilization. *J. Biol. Chem. 277*, 41032−41037.
(42) Olshina, M. A., Angley, L. M., Ramdzan, Y. M., Tang, J., Bailey, M. F., Hill, A. F., and Hatters, D. M. (2010) Tracking mutant huntingtin aggregation kinetics in cells reveals three major populations that include an invariant oligomer pool. *J. Biol. Chem. 285*, 21807−21816.
(43) Nucifora, L. G., Burke, K. A., Feng, X., Arbez, N., Zhu, S., Miller, J., Yang, G., Ratovitski, T., Delannoy, M., Muchowski, P. J., Finkbeiner, S., Legleiter, J., Ross, C. A., and Poirier, M. A. (2012) Identification of novel potentially toxic oligomers formed in vitro from mammalian-derived expanded huntingtin exon-1 protein. *J. Biol. Chem. 287*, 16017−16028.
(44) Gu, X., Greiner, E. R., Mishra, R., Kodali, R., Osmand, A., Finkbeiner, S., Steffan, J. S., Thompson, L. M., Wetzel, R., and Yang, X. W. (2009) Serines 13 and 16 are critical determinants of full-length human mutant huntingtin induced disease pathogenesis in HD mice. *Neuron 64*, 828−840.
(45) Sivanandam, V. N., Jayaraman, M., Hoop, C. L., Kodali, R., Wetzel, R., and van der Wel, P. C. (2011) The aggregation-enhancing huntingtin N-terminus is helical in amyloid fibrils. *J. Am. Chem. Soc. 133*, 4558−4566.
(46) Jayaraman, M., Mishra, R., Kodali, R., Thakur, A. K., Koharudin, L. M., Gronenborn, A. M., and Wetzel, R. (2012) Kinetically competing huntingtin aggregation pathways control amyloid polymorphism and properties. *Biochemistry 51*, 2706−2716.
(47) Mishra, R., Hoop, C. L., Kodali, R., Sahoo, B., van der Wel, P. C., and Wetzel, R. (2012) Serine phosphorylation suppresses huntingtin amyloid accumulation by altering protein aggregation properties. *J. Mol. Biol. 424*, 1−14.
(48) Mishra, R., Jayaraman, M., Roland, B. P., Landrum, E., Fullam, T., Kodali, R., Thakur, A. K., Arduini, I., and Wetzel, R. (2012) Inhibiting the nucleation of amyloid structure in a huntingtin fragment by targeting alpha-helix-rich oligomeric intermediates. *J. Mol. Biol. 415*, 900−917.
(49) Burke, K. A., Kauffman, K. J., Umbaugh, C. S., Frey, S. L., and Legleiter, J. (2013) The interaction of polyglutamine peptides with lipid membranes Is regulated by flanking sequences associated with huntingtin. *J. Biol. Chem. 288*, 14993−15005.
(50) Crick, S. L., Ruff, K. M., Garai, K., Frieden, C., and Pappu, R. V. (2013) Unmasking the roles of N- and C-terminal flanking sequences from exon 1 of huntingtin as modulators of polyglutamine aggregation. *Proc. Natl. Acad. Sci. U.S.A. 110*, 20075−20080.
(51) Wacker, J. L., Zareie, M. H., Fong, H., Sarikaya, M., and Muchowski, P. J. (2004) Hsp70 and Hsp40 attenuate formation of spherical and annular polyglutamine oligomers by partitioning monomer. *Nat. Struct. Mol. Biol. 11*, 1215−1222.
(52) Williamson, T. E., Vitalis, A., Crick, S. L., and Pappu, R. V. (2010) Modulation of polyglutamine conformations and dimer formation by the N-terminus of huntingtin. *J. Mol. Biol. 396*, 1295−1309.
(53) Singer, D., Zauner, T., Genz, M., Hoffmann, R., and Zuchner, T. (2010) Synthesis of pathological and nonpathological human exon 1 huntingtin. *J. Pept. Sci. 16*, 358−363.
(54) O'Nuallain, B., Thakur, A. K., Williams, A. D., Bhattacharyya, A. M., Chen, S., Thiagarajan, G., and Wetzel, R. (2006) Kinetics and thermodynamics of amyloid assembly using a high-performance liquid chromatography-based sedimentation assay. *Methods Enzymol. 413*, 34−74.
(55) Chemuru, S., Kodali, R., and Wetzel, R. (2014) Improved chemical synthesis of hydrophobic Abeta peptides using addition of C-terminal lysines later removed by carboxypeptidase B. *Biopolymers 102*, 206−221.
(56) Kar, K., Jayaraman, M., Sahoo, B., Kodali, R., and Wetzel, R. (2011) Critical nucleus size for disease-related polyglutamine aggregation is repeat-length dependent. *Nat. Struct. Mol. Biol. 18*, 328−336.
(57) Quillin, M. L., and Matthews, B. W. (2000) Accurate calculation of the density of proteins. *Acta Crystallogr., Sect. D: Biol. Crystallogr. 56*, 791−794.
(58) Haris, P. I., and Chapman, D. (1995) The conformational analysis of peptides using Fourier transform IR spectroscopy. *Biopolymers 37*, 251−263.
(59) O'Nuallain, B., Williams, A. D., Westermark, P., and Wetzel, R. (2004) Seeding specificity in amyloid growth induced by heterologous fibrils. *J. Biol. Chem. 279*, 17490−17499.
(60) O'Nuallain, B., Shivaprasad, S., Kheterpal, I., and Wetzel, R. (2005) Thermodynamics of abeta(1−40) amyloid fibril elongation. *Biochemistry 44*, 12709−12718.
(61) Williams, A. D., Shivaprasad, S., and Wetzel, R. (2006) Alanine scanning mutagenesis of Abeta(1−40) amyloid fibril stability. *J. Mol. Biol. 357*, 1283−1294.
(62) Kodali, R., Williams, A. D., Chemuru, S., and Wetzel, R. (2010) Abeta(1−40) forms five distinct amyloid structures whose beta-sheet contents and fibril stabilities are correlated. *J. Mol. Biol. 401*, 503−517.
(63) Kar, K., Hoop, C. L., Drombosky, K. W., Baker, M. A., Kodali, R., Arduini, I., van der Wel, P. C., Horne, W. S., and Wetzel, R. (2013) beta-hairpin-mediated nucleation of polyglutamine amyloid formation. *J. Mol. Biol. 425*, 1183−1197.
(64) Bugg, C. W., Isas, J. M., Fischer, T., Patterson, P. H., and Langen, R. (2012) Structural features and domain organization of huntingtin fibrils. *J. Biol. Chem. 287*, 31739−31746.
(65) Bhattacharyya, A., Thakur, A. K., Chellgren, V. M., Thiagarajan, G., Williams, A. D., Chellgren, B. W., Creamer, T. P., and Wetzel, R. (2006) Oligoproline effects on polyglutamine conformation and aggregation. *J. Mol. Biol. 355*, 524−535.
(66) Martin-Aparicio, E., Yamamoto, A., Hernandez, F., Hen, R., Avila, J., and Lucas, J. J. (2001) Proteasomal-dependent aggregate reversal and absence of cell death in a conditional mouse model of Huntington's disease. *J. Neurosci. 21*, 8772−8781.
(67) Orr, H. T. (2004) Neurodegenerative disease: Neuron protection agency. *Nature 431*, 747−748.
(68) Sathasivam, K., Lane, A., Legleiter, J., Warley, A., Woodman, B., Finkbeiner, S., Paganetti, P., Muchowski, P. J., Wilson, S., and Bates, G. P. (2010) Identical oligomeric and fibrillar structures captured from the brains of R6/2 and knock-in mouse models of Huntington's disease. *Hum. Mol. Genet. 19*, 65−78.
(69) Wetzel, R., and Goeddel, D. V. (1983) Synthesis of polypeptides by recombinant DNA methods, In *The Peptides: Analysis, Synthesis, Biology* (Meienhofer, J., and Gross, E., Eds.), pp 1−64, Academic Press, New York.
(70) Finder, V. H., Vodopivec, I., Nitsch, R. M., and Glockshuber, R. (2010) The recombinant amyloid-beta peptide Abeta1−42 aggregates faster and is more neurotoxic than synthetic Abeta1−42. *J. Mol. Biol. 396*, 9−18.
(71) Scherzinger, E., Lurz, R., Turmaine, M., Mangiarini, L., Hollenbach, B., Hasenbank, R., Bates, G. P., Davies, S. W., Lehrach, H., and Wanker, E. E. (1997) Huntingtin-encoded polyglutamine

expansions form amyloid-like protein aggregates in vitro and in vivo. *Cell 90*, 549−558.
(72) Burke, K. A., Hensal, K. M., Umbaugh, C. S., Chaibva, M., and Legleiter, J. (2013) Huntingtin disrupts lipid bilayers in a polyQ-length dependent manner. *Biochim. Biophys. Acta: Biomembr. 1828*, 1953−1961.
(73) Ansaloni, A., Wang, Z. M., Jeong, J. S., Ruggeri, F. S., Dietler, G., and Lashuel, H. A. (2014) One-Pot Semisynthesis of Exon 1 of the Huntingtin Protein: New Tools for Elucidating the Role of Posttranslational Modifications in the Pathogenesis of Huntington's Disease. *Angew. Chem., Int. Ed. 53*, 1928−1933.
(74) Chen, S., Ferrone, F., and Wetzel, R. (2002) Huntington's Disease age-of-onset linked to polyglutamine aggregation nucleation. *Proc. Natl. Acad. Sci. U.S.A. 99*, 11884−11889.